Properties of the Experimental Crystal Charge Density of Methylammonium Hydrogen Maleate. A Salt with a Very Short Intramolecular O−H−O Hydrogen Bond

Dennis Madsen,† Claus Flensburg, and Sine Larsen*

Centre for Crystallographic Studies, Department of Chemistry, University of Copenhagen, Universitetsparken 5, DK-2100 Copenhagen Ø, Denmark

Received: July 24, 1997; In Final Form: November 19, 1997

The experimental crystal charge density of deuterated methylammonium hydrogen maleate has been determined from neutron and X-ray diffraction data collected at 122.4 K. Refinements of the neutron diffraction data showed that the very short intramolecular O−H−O hydrogen bonds found in the two independent anions are symmetric with D(H) on crystallographic mirror planes. The experimental charge density was subjected to a topological analysis. It is positive throughout the unit cell and constitutes a topological space that fulfills the Poincaré−Hopf relation. The topological analysis enabled us to characterize different types of interatomic interactions in the crystal and showed that the two very short intramolecular hydrogen bonds have covalent character. Newly developed algorithms made it possible to determine the atomic basins in the crystal charge density, which were used to calculate integrated properties such as volume, charge, and the integrated Laplacian. Those of the methylammonium ion have been compared with the corresponding topological properties of the same cation in its hydrogen succinate salt. All the properties were quantitatively transferable, a strong indication that transferability can also be applied to experimentally determined electron densities.

Introduction

The characteristics of theoretical charge densities in terms of topological properties and critical points have been employed by Bader to provide insight into the interatomic interactions in molecules.[1] It has recently been shown that experimental electron densities obtained from accurate X-ray diffraction data subjected to a similar analysis can provide valuable information on interatomic interactions in crystals.[2−6]

Strong and short O−H−O hydrogen bonds with O−O distances less than 2.50 Å are found in a variety of systems, and the promotion of proton transfer in such short hydrogen bonds is of significance from materials science to biochemistry. A recent study of the quantum nature of charged water complexes showed that the proton-transfer properties depend significantly on the O−O distance.[7] Geometrical data for short O−H−O hydrogen-bonded systems have been used by Gilli et al. to derive an empirical description of the bonding properties of very short O−H−O hydrogen bonds, which made them conclude that these interactions are covalent in nature.[8] However it is apparent from their analysis that the short symmetric hydrogen bonds, that are found between a carboxylic acid and a carboxylate group are described less well by the derived empirical parameters. Such short hydrogen bonds that are observed in acid salts of dicarboxylic acids were thoroughly analyzed by Speakman.[9] He found that in compounds with short O−H−O hydrogen bonds, e.g. O−O distances less than 2.45 Å, it is frequently seen that the two oxygen atoms are related by crystallographic symmetry. It is quite common for these systems that they crystallize in space groups that are not uniquely determined from their systematic absences. It is exclusively the position of the hydrogen atom in the symmetric hydrogen bond that determines whether the space group is centric with the hydrogen atom on a crystallographic symmetry element or acentric with a disordered hydrogen atom. For such compounds, a neutron diffraction study is essential to establish the correct space group before the experimental charge density obtained from X-ray diffraction data can be thoroughly analyzed.

The neutron diffraction study of methylammonium hydrogen succinate monohydrate (MAHS) verified that the very short hydrogen bond that links different anions is symmetric, with the hydrogen at a crystallographic inversion center.[3] The experimental charge distribution of that salt was subjected to a topological analysis, which showed that the very short symmetric O−H−O hydrogen bond possesses distinct covalent character. Very short O−H−O hydrogen bonds are also observed in acid salts of maleic acids, but because of the cis configuration of the acid, an intramolecular O−H−O hydrogen bond is formed with O−O distances of ca. 2.42 Å. In the hydrogen maleate salts it is also common that the anion is found on crystallographic mirror planes. An indication of the special character of this intramolecular hydrogen bond can be found in the difference between the p*K* values of maleic acid and fumaric acid, the corresponding trans isomer of maleic acid. The two p*K* values differ by 4.14 for maleic acid and by 1.39 for fumaric acid, which indicates that the intramolecular hydrogen bond contributes to the stability of the hydrogen maleate ion.

We found that methylammonium hydrogen maleate (MADMA) was very suitable for a topological study of the experimental charge density. A previous X-ray diffraction study based on data to a fairly high resolution verified that this compound crystallizes in either $Pna2_1$ or its centric equivalent space group *Pnam* with eight formula units in the unit cell.[10] In the centric model the structure contains one independent methylammonium ion and two crystallographically independent hydrogen maleate ions on crystallographic mirror planes. The X-ray diffraction study showed that the best agreement with the experimental

* Author to whom correspondence should be addressed. E-mail: sine@xray.ki.ku.dk.

† Present address: ESRF, BP 220, 38043 Grenoble Cedex, France.

S1089-5639(97)02419-5 CCC: $15.00
Published on Web 03/19/1998

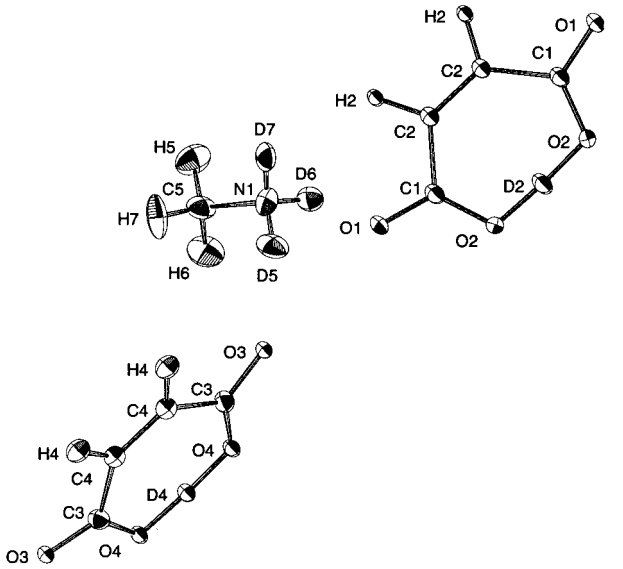

Figure 1. ORTEP drawing of the entities in MADMA showing 50% probability ellipsoids. The ellipsoids for the C, N, and O atoms are drawn using the X-ray parameters, and the H/D ellipsoids are drawn using the scaled neutron parameters (cf. the subsection Displacement Parameters).

data was found in the centric space group. An ORTEP[11] drawing of the entities found in the crystal are shown in Figure 1. We present here the results obtained from a neutron diffraction study and a new set of high-resolution X-ray diffraction data.

The methylammonium ion was also used as the counterion in the hydrogen succinate salt, whose experimental charge density had been subjected to a similar investigation. This makes it possible to examine the transferability between different experimental charge densities, as the hydrogen bond interactions in the two methylammonium salts are quite different. Besides the unique very short O−H−O intramolecular hydrogen bonds in the hydrogen maleate, this charge density study will also provide information on different types of intermolecular interactions.

Experimental Section

Methylammonium hydrogen maleate was prepared as previously described.[10] The deuterated crystals used for the neutron and X-ray experiments were prepared by slow evaporation of a solution of methylammonium hydrogen maleate in CH_3CH_2-OD kept in a desiccator at room temperature. The crystals used for both data collections were selected from the same batch and were therefore assumed to have the same H/D isotope composition.

Data Collections

Neutron Diffraction Data. The neutron diffraction data set was collected at Risø National Laboratory on the four-circle diffractometer at the DR3 reactor. A Be(002) monochromator was used to select neutrons with a wavelength of 1.047 Å. The phase transition of KH_2PO_4 at 122.4 K was used to calibrate the reading of the Pt-thermometer.[12] A single crystal of KH_2PO_4 mounted in a Displex cryostat was used for the adjustment. Methylammonium hydrogen maleate grows as elongated prisms; we selected a single crystal with dimensions 4.0 × 3.1 × 1.1 mm bound by the forms {0 1 0}, {1 0 0}, and {0 1 $\bar{1}$}. It was mounted in the Displex cryostat, and the temperature set to 122.4 K. The orientation matrix and unit cell parameters were determined from setting angles for more than 50 reflections. An $\omega-2\theta$ step scan was employed to record the profiles of the reflections. A total measuring time of 8 min was used per reflection to record 48 equally spaced steps. The temperature was noted for each reflection, and the variation was within 0.5 K during the data collection. Three standard reflections, (0 0 4), (0 2 0), and (2 0 0), were measured every 100 reflections, and the variation of their intensities was less than 1% during the three weeks of data collection. Additional details concerning the neutron data collection are given in Table 1.

TABLE 1: Summary of Experimental Details and Refinement Results for the Neutron and X-ray Diffraction Measurements on Deuterated Methylammonium Hydrogen Maleate, Space Group *Pnam* (Nonstandard Setting of *Pnma* [No. 62])

	X-ray	neutron
a/Å	6.427(1)	6.41(2)
b/Å	11.826(2)	11.81(3)
c/Å	17.616(2)	17.67(4)
wavelength/Å	0.71073	1.047
temperature/K	122.4(5)	122.4(5)
μ/mm^{-1}	0.13	0.00132
crystal size/mm	0.40 × 0.25 × 0.25	4.0 × 3.1 × 1.1
scan type	$\omega-2\theta$	$\omega-2\theta$
$(\sin\theta/\lambda)_{max}$/Å^{-1}	1.08	0.73
indices range		
h	−4→15	0→9
k	−27→28	0→17
l	−40→42	0→25
no. of reflections		
measured	31455	2958
independent	7192	2067
R_{int} ($\|F\|^2$)	0.0246	0.0137
S^a	1.1019	4.07
no. of variables	343	178
$R(\|F\|)^b$	0.0411	0.0773
$wR(\|F\|)^c$	0.0161	0.0557
$R(\|F\|^2)^b$	0.0195	0.0797
$wR(\|F\|^2)^c$	0.0298	0.0954

a

$$S = \sqrt{\frac{\sum_{\bar{h}} w_{\bar{h}}(|F_c(\bar{h})|^2 - k|F_o(\bar{h})|^2)^2}{m-p}}$$

b

$$R(|F|^n) = \frac{\sum_{\bar{h}}(|F_c(\bar{h})|^n - k|F_o(\bar{h})|^n)^2}{\sum_{\bar{h}}(|F_o(\bar{h})|^n)^2}$$

c

$$wR(|F|^n) = \frac{\sum_{\bar{h}} w_{\bar{h}}(|F_c(\bar{h})|^n - k|F_o(\bar{h})|^n)^2}{\sum_{\bar{h}} w_{\bar{h}}(|F_o(\bar{h})|^n)^2}$$

$$w_{\bar{h}} = 1/\sigma^2(|F_o(\bar{h})|^n)$$

In these definitions *m* is the number of measurements and *p* the number of parameters in the model.

X-ray Diffraction Data. The X-ray diffraction data set was collected on an Enraf-Nonius CAD4 diffractometer with a Mo Kα X-ray tube and a graphite monochromator. The temperature was controlled with a gas flow low-temperature device adjusted to 122.4 K with the phase transition of KH_2PO_4. The temperature variation during the data collection was less than 0.5 K. Several crystals were examined on the diffractometer. On the basis of the criteria of sharp well-defined reflection profiles and scattering to a high resolution, the best crystal was selected that had dimensions 0.40 × 0.25 × 0.25 mm. The orientation matrix and unit cell parameters were determined from setting angles of 20 reflections with θ between 19° and 21°. The scan range $\Delta\theta$ was set to 1.00 + 0.35 tan θ on the basis of an analysis of

the profiles for several reflections. A half-sphere of data was collected to $\theta = 50°$. The orientation of the crystal was checked for every 600 reflections by measurement of the setting angles for seven reflections. The orientation of the crystal did not change during the data collection. Five standard reflections, (2 0 0), (1 $\bar{2}$ 0), (2 1 1), (0 0 10), and (6 0 $\bar{1}$), were measured every 2.7 h during the data collection lasting two months. The variation in the intensities of these reflections is discussed in the data reduction section.

A preliminary refinement with SHELXL-93[13] of the X-ray data set showed a rather low F_o^2/F_c^2 ratio of the (2 0 0) reflection; therefore some experiments were conducted to find the origin of this discrepancy. A data collection of the reflections with Bragg angles below 15° was carried out with the power from the X-ray tube turned down to one-fourth to check for overload of the detector. The measurements with full power and the measurements with one-fourth power scaled together without any systematic variation, between strong and weak reflections, which excluded overload of the detector as a cause of this variation. ψ-scans of the three reflections with the lowest F_o^2/F_c^2 ratios did not show any sign of multiple reflection. The phenomenon was therefore concluded to originate in extinction, and the intensity variations of the ψ-scans were sufficiently small to make an isotropic correction a suitable model. Further details concerning the X-ray data collection are shown in Table 1.

Data Reduction

The processing of both the neutron and X-ray diffraction data was performed with the DREADD program package.[14]

Neutron Data. The neutron data set was corrected for background and Lorentz effects. The absorption in the neutron experiment was negligible for the single crystal used (transmission factors of 0.999), and thus no absorption correction was performed. The 2958 measured reflections were averaged to 2067 unique with $R_{int}(|F|^2) = 0.0137$. Of these, more than 85% had intensities above 4 su. The standard uncertainties of the squared structure factors were based on the counting statistics.

X-ray Data. The X-ray data were corrected for background, polarization, and Lorentz effects. Absorption correction was not considered necessary. Refinements were carried out using data with and without correction for thermal diffuse scattering (TDS). The two refinements gave identical displacement parameters, within the standard uncertainty, and therefore the data not corrected for TDS were used in the refinements.

The averaging of the X-ray diffraction data became somewhat complicated because of a shutdown of the cooling system for a couple of hours after six weeks of data collection. The shutdown resulted in a heating of the crystal to room temperature and a subsequent cooling to 122.4 K. All five standard reflections showed a linear decay prior to the heating and cooling of the crystal, which can be attributed to the decay in the intensity from the X-ray tube. The intensities of the standard reflections had a very different behavior after the heating and cooling of the crystal. The intensities of the two strongest (low order) reflections showed a discontinuity associated with the heating and cooling of the crystal, whereas the other three had a linear decay during the whole data collection. We attributed the sudden change in intensity to a change in the mosaicity of the crystal due to the heating and cooling. The measurements were therefore divided into two data sets: one including data before the heating and cooling of the crystal and the other the rest of the reflections. Reflections with θ between 0° and 15° were remeasured four times after the shutdown of the cooling device, as their intensities were expected to be most affected by the change in mosaicity, and measurements of the same reflections prior to the shutdown were excluded. The two data sets were individually corrected for the linear decay with small relative errors (0.2% and 0.6%), and the two data sets could be scaled together with a very small relative error (0.1%). These 31 455 selected reflections were averaged to give 7192 unique with $R_{int}(|F|^2) = 0.0246$, and the data set was concluded to be of a sufficient quality for a charge density analysis. The standard uncertainties of the squared structure factors were calculated statistically from the variation of the individual (≥ 4) measurements for each reflection. Of the 7192 unique reflections, 70% had intensities above 4 su.

Least-Squares Refinements

The program VALRAY[15] was used for the least-squares refinements of both the neutron and X-ray data sets. The quantity minimized in both cases was $\sum w_{\bar{h}}(|F_o(\bar{h})|^2 - k|F_c(\bar{h})|^2)^2$, the weights employed were $w_{\bar{h}} = 1/\sigma^2(|F_o(\bar{h})|^2)$, and all reflections were included in the summations. Throughout the refinements we used Hamiltons ratio test[16] to evaluate the significance of introducing new parameters in the model.

Refinement of Neutron Data. In the refinement of the neutron data the scattering lengths used were $b_C = 6.648$, $b_H = -3.741$, $b_D = 6.674$, $b_O = 5.805$, and $b_N = 9.300$ fm.[17] The scattering lengths for the two types of hydrogen atoms exchanged by deuteration were included in the refinement, i.e. those of the ammonium group and the short hydrogen bonds.

The previous X-ray study did not enable us to decide unambiguously whether *Pnam* or $Pna2_1$ is the correct space group.[10] Therefore refinements were performed in both space groups. The positional parameters resulting from the refinement in $Pna2_1$ correspond within the standard uncertainty to the centric model, and the parameters of C(2) and C(2)′ were strongly correlated. When the atoms D(2) and D(4), which take part in the two short hydrogen bonds, were excluded from the acentric model, two peaks were found in the nuclear difference density, both in the center of a short hydrogen bond. Refinement with D(2) and D(4) fixed in the crystallographic mirror planes resulted in anisotropic displacement parameters for D(2) and D(4) similar in magnitude to those of the other hydrogen atoms in the structure. Within the accuracy of the neutron data, these results demonstrate that a center of inversion is present in the crystal. This implies that the correct space group is *Pnam* and that very short symmetric hydrogen bonds are found in both hydrogen maleate ions. Inclusion of third-order Gram−Charlier parameters did not improve the model significantly, and none of these new parameters had values above 2 su. The nuclear density distribution was therefore modeled by a harmonic model with anisotropic displacement parameters.

The final model for the neutron data consisted of 178 parameters that included positional and anisotropic displacement parameters for all atoms and an isotropic extinction parameter (g) according to the Becker and Coppens model[18] with a Lorentzian distribution of the mosaic blocks. The parameter refined to a value of $18.5(8) \times 10^{-4}$ rad^2 with the lowest F_o^2/F_c^2 ratio of 0.788 for the (2 0 0) reflection. The population of deuterium was 0.820(4) in the ammonium group and 0.639(4) in the short intramolecular hydrogen bonds. The residuals from the final neutron model are listed in Table 1 and the resulting parameters in Tables 2 and 3.

Refinement of X-ray Data. The positional parameters for the H/D atoms were fixed to the values from the refinement of the neutron data during the refinements of the X-ray data. The

TABLE 2: Atomic Positions in Fractional Coordinates[a]

atom	*x*	*y*	*z*
O(1)	0.15258(6)	0.58582(3)	0.08992(1)
	0.1528(4)	0.5856(2)	0.0900(1)
O(2)	0.00019(6)	0.68421(3)	0.18127(2)
	0.007(4)	0.6843(2)	0.1815(1)
O(3)	0.26698(6)	0.16805(3)	0.08847(2)
	0.2667(4)	0.1681(2)	0.0885(1)
O(4)	0.26169(6)	0.29467(2)	0.18136(2)
	0.2616(4)	0.2944(2)	0.1815(1)
N(1)	0.18233(5)	0.37148(3)	0.01101(2)
	0.1825(2)	0.3716(1)	0.0111(1)
C(1)	0.13843(4)	0.61436(2)	0.15777(1)
	0.1382(3)	0.6141(1)	0.1577(1)
C(2)	0.28968(4)	0.56268(2)	0.21186(1)
	0.2897(3)	0.5627(1)	0.2118(1)
C(3)	0.27071(4)	0.19215(2)	0.15715(1)
	0.2709(3)	0.1921(1)	0.1572(1)
C(4)	0.28616(4)	0.09589(2)	0.21184(1)
	0.2862(3)	0.0959(1)	0.2118(1)
C(5)	0.13802(6)	0.88543(3)	0.04076(2)
	0.1389(3)	0.8851(1)	0.0407(1)
D(2)	0.0023(11)	0.6907(6)	1/4
D(4)	0.2618(11)	0.2985(6)	1/4
H(2)	0.4113(7)	0.5149(4)	0.1840(3)
H(4)	0.2992(8)	0.0145(3)	0.1837(2)
D(5)	0.0447(5)	0.3734(3)	−0.0198(2)
D(6)	0.1775(5)	0.4365(3)	0.0496(2)
D(7)	0.1945(5)	0.2960(3)	0.0408(2)
H(5)	−0.0042(7)	0.8766(4)	0.0090(3)
H(6)	0.1454(9)	0.9686(4)	0.0665(3)
H(7)	0.1472(9)	0.8213(5)	0.0848(3)

[a] The first line for the C, N, and O atoms are from the X-ray multipole refinements and the second line from the refinement of the neutron data. The positions of the H/D atoms are from the refinement of the neutron data.

anisotropic displacement parameters for the H/D atoms were not varied during the X-ray refinements and initially set to the neutron values. In the final refinement the *U* tensors of the H/D atoms were scaled due to truncation errors in the neutron data set, vide infra.

A refinement with third-order Gram−Charlier coefficients on the C, N, and O atoms resulted in significant negative peaks in the electron density near the lone-pair regions on the O atoms, and the third-order Gram−Charlier coefficients had all values below 3 su. Therefore we preferred the model with anisotropic displacement parameters on the C, N, and O atoms.

The initial model consisted of 336 parameters, which included positional and anisotropic displacement parameters for the C, N, and O atoms and an isotropic extinction parameter (*g*) according to Becker and Coppens[18] with Lorentzian distribution of the mosaic blocks. The electron density was modeled by the following set of multipole parameters:[19] monopole, dipole, and quadrupole parameters on all atoms and octopole parameters on the C, N, and O atoms. The D_z, Q_{xz}, and Q_{yz} parameters were constrained to zero for the two H/D atoms with site symmetry *m*. The core monopole populations on the C, N, and O atoms were constrained to be equal (p_c(C) = p_c (N) = p_c(O)). The scale factor was not varied, in these refinements, but calculated as the ratio between the sum of the core and valence monopole populations and *F*(000).[20]

The radial functions on the monopole, dipole, and quadrupole functions for the C, N, and O atoms were the density-localized[21] orbital products of Clementi and Roetti.[22] Using (is) to symbolize inner shell density localized orbital product and (os) for the outer shell products, the following products were used as radial functions: core monopoles (is)(is), valence monopoles (os)(os), dipoles (os)(2p), and quadrupoles (2p)(2p). The representations of the radial functions for the H/D atoms and for the octopole level on the other atom types were Slater-type exponentials, $r^n \exp(-\alpha r)$. The initial radial scaling parameters were the standard molecular values: $\alpha_{H/D} = 2.48$, $\alpha_C = 3.44$, $\alpha_N = 3.90$, and $\alpha_O = 4.50$ Å^{-1}.[23] The exponents *n* were set to the orbital quantum number *l*. Allowing these radial scaling parameters to vary in the refinement was a significant improvement of the model. The seven new parameters were as follows: one common α parameter on the radial functions for the H/D atoms; one common κ parameter for the valence monopole, dipole, and quadrupole radial functions; and one α parameter for the octopole function for each of the other three atom types. Increasing the number of freely variable radial scaling parameters did not improve the agreement with the observed structure amplitudes.

Displacement Parameters. The final displacement parameters derived from the refinements of the neutron and X-ray data sets showed discrepancies for the C, N, and O atoms, as shown in Table 3.

An examination of the reflection profiles in the neutron data showed that the scan range had been too narrow for some reflections. This would be expected to affect the displacement parameters most. Blessing[24] has suggested a linear model to scale the two sets of displacement parameters:

$$U_{ij}(\mathrm{N}) = a_{ij} + b_{ij}U_{ij}(\mathrm{X})$$

where U_{ij}(N) is the neutron value and U_{ij}(X) the X-ray value. The anisotropic displacement parameters for C, N, and O in Table 3 were used to obtain the six least-squares lines shown in Figure 2. The standard uncertainties of the displacement parameters were used in the calculation of the uncertainties of the least-squares parameters, a_{ij} and b_{ij}. The anisotropic displacements parameters of the H/D atoms obtained from the neutron refinement were subsequently scaled using these parameters.

Final X-ray Model. The final X-ray model included 343 parameters, the corresponding residuals are listed in Table 1, and the positional parameters are given in Table 2. The extinction parameter (*g*) refined to a value of $1.28(2) \times 10^{-4}$ rad^2 with the lowest F_o^2/F_c^2 ratio of 0.73 for the (2 0 0) reflection. The estimated scale factor was 0.9975(24). The radial scaling parameters refined to the values $k_C = 1.014(3)$, $k_N = 1.001(4)$, $k_O = 0.981(1)$, $\alpha_{H/D} = 4.43(3)$, $\alpha_C = 5.87(6)$, $\alpha_N = 6.9(2)$, and $\alpha_O = 7.6(4)$ Å^{-1}. The final difference map was featureless. A map of the region around one of the anions is provided as part of the Supporting Information.

Results and Discussion

The refinements of the neutron diffraction data showed unambiguously that the correct space group for methylammonium hydrogen maleate is *Pnam*, a nonstandard setting of the space group *Pnma* (no. 62). The cations and anions in the unit cell possess different site symmetry. Whereas the methylammonium ion is in a general position, the two crystallographically independent hydrogen maleate ions are found on crystallographic mirror planes bisecting the C═C bonds and the two short hydrogen bonds with O···O distances O(2)···O(2)′ = 2.4214(5) Å and O(4)···O(4)′ = 2.4183(5) Å. Besides these very short intramolecular hydrogen bonds, weaker hydrogen bonds connect the methylammonium ions to the different hydrogen maleate ions as shown by the stereo pair in Figure 3,

TABLE 3: Anisotropic Displacement Parameters in Å^2 [a]

atom	U_{11}	U_{22}	U_{33}	$.U_{12}$	U_{13}	U_{23}
O(1)	0.01884(11)	0.02157(10)	0.00964(9)	0.00233(11)	−0.00132(8)	−0.00193(8)
	0.0191(9)	0.0262(10)	0.0170(8)	0.0031(8)	−0.0015(8)	−0.0013(7)
O(2)	0.01931(11)	0.01919(10)	0.01166(9)	0.00764(9)	0.00125(8)	0.00056(8)
	0.0203(9)	0.0259(10)	0.0174(9)	0.0074(10)	−0.007(8)	0.000(8)
O(3)	0.02501(13)	0.01830(11)	0.01005(9)	0.00099(10)	−0.00011(7)	−0.00036(9)
	0.0257(10)	0.0224(9)	0.0180(9)	−0.0001(9)	−0.0010(8)	−0.0002(8)
O(4)	0.02398(13)	0.01226(9)	0.01170(9)	0.00067(9)	−0.00036(7)	0.00085(8)
	0.0229(10)	0.0163(8)	0.0199(8)	0.0011(8)	−0.0002(8)	0.002(7)
N(1)	0.01653(11)	0.01805(9)	0.01148(8)	0.00120(12)	−0.00092(9)	0.00019(8)
	0.0169(5)	0.0216(5)	0.0184(5)	0.0007(5)	−0.0010(5)	−0.0002(5)
C(1)	0.01374(9)	0.01424(8)	0.00884(8)	0.00084(8)	−0.00032(7)	−0.00038(7)
	0.0144(7)	0.0177(8)	0.0166(7)	0.0020(7)	−0.0003(6)	−0.0004(6)
C(2)	0.01331(9)	0.01621(8)	0.00978(7)	0.00288(10)	0.00007(6)	−0.00007(8)
	0.0139(7)	0.0203(7)	0.0171(7)	0.0019(7)	−0.0007(7)	0.0004(6)
C(3)	0.01515(9)	0.01322(7)	0.00950(7)	0.00048(9)	−0.00002(6)	0.00000(8)
	0.0147(7)	0.0168(7)	0.0173(7)	0.0001(6)	0.0001(6)	0.0006(6)
C(4)	0.01556(10)	0.01137(7)	0.01073(7)	0.00159(8)	0.00006(6)	−0.00065(8)
	0.0153(6)	0.0158(7)	0.0186(6)	0.0010(6)	0.0005(7)	0.0001(6)
C(5)	0.01939(12)	0.01646(10)	0.01617(11)	0.00035(10)	0.00201(9)	0.00038(10)
	0.0184(7)	0.0210(8)	0.0236(8)	−0.0001(7)	0.0016(8)	0.0012(7)
D(2)	0.026(3)	0.026(3)	0.025(3)	0.007(3)	0	0
	0.026	0.022	0.018	0.007	0	0
D(4)	0.023(3)	0.018(3)	0.032(3)	−0.001(2)	0	0
	0.023	0.014	0.025	−0.002	0	0
H(2)	0.027(2)	0.053(3)	0.036(2)	0.015(2)	0.004(2)	−0.002(2)
	0.027	0.046	0.029	0.014	0.005	−0.005
H(4)	0.047(2)	0.026(2)	0.033(2)	0.003(2)	−0.004(2)	−0.005(1)
	0.048	0.021	0.026	0.003	−0.005	−0.008
D(5)	0.024(1)	0.038(2)	0.031(2)	0.001(1)	−0.004(1)	−0.001(2)
	0.023	0.032	0.025	0.001	−0.005	−0.001
D(6)	0.030(2)	0.037(1)	0.028(1)	0.006(1)	0.000(1)	−0.009(1)
	0.030	0.031	0.021	0.006	0.000	−0.012
D(7)	0.028(1)	0.035(1)	0.033(1)	−0.002(1)	0.001(1)	0.009(1)
	0.028	0.029	0.027	−0.001	0.001	0.013
H(5)	0.026(2)	0.046(2)	0.059(2)	−0.001(2)	−0.002(2)	−0.005(3)
	0.026	0.040	0.054	0.001	−0.004	−0.007
H(6)	0.053(3)	0.038(2)	0.049(3)	0.006(2)	0.006(2)	−0.014(2)
	0.055	0.033	0.043	0.006	0.007	−0.020
H(7)	0.052(3)	0.055(3)	0.042(2)	0.005(3)	0.013(2)	0.019(2)
	0.054	0.048	0.036	0.005	0.016	0.026

[a] The first line for the C, N, and O atoms represent the X-ray and the second line the neutron parameters. For the H/D atoms the first line is the unscaled values from the neutron refinement and the second line is the scaled value.

forming alternating layers of cations and anions in the direction of the *c*-axis.

The hydrogen maleate ions have slightly different conformations; the molecular plane of anion 2 (C(3), C(4), O(3), O(4), H(4), and D(4)) is almost parallel to the crystal *bc*-plane and is also the more planar. The torsion angle O(3)−C(3)−C(4)−C(4)′ is 177.48(3)°; the equivalent angle in the other anion differs by 10°, 167.65(3)°. All the geometrical features involving the non-hydrogen atoms, bond lengths, bond angles, and torsion angles, derived from the multipole model compare extremely well with the values reported earlier from a conventional refinement using another high-resolution data set.[10]

An X−N deformation study based on room-temperature data has previously been performed for both imididazolium and calcium hydrogen maleate.[25] The features of the deformation density of the hydrogen maleate ion in these two structures are qualitatively in agreement with the deformation densities of the two hydrogen maleate ions in MADMA, depicted in Figure 4, which show the static deformation maps ($\rho_{model} - \rho_{IAM}$) calculated through the plane of the carbon atoms. They are very similar with respect to the size and shape of the bonding and lone-pair densities and contain significantly more details especially in the lone-pair regions than the deformation densities reported in the earlier room-temperature study.[25] To obtain more quantitative measures of the properties of the experimental crystal charge density of methylammonium hydrogen maleate, a topological analysis was performed.

Topology of the Crystal Electron Density. The total electron density carries a wealth of information about the physical properties of the system, and Bader has demonstrated how the interatomic interactions in a system can be characterized quantitatively by a topological analysis of the quantum chemical electron density.[1] It relies on the localization of the critical points in the electron density, i.e. points with zero gradient of the electron density, $\nabla\rho(\mathbf{r}_c) = 0$. Besides the position of the critical point and the corresponding value of the electron density, the second derivatives, i.e., the Hessian matrix, characterize the critical point. The number of its nonzero eigenvalues defines the rank, *r*, and the algebraic sum of the eigenvalues its signature, *s*. The nomenclature (*r*,*s*) is used to classify a given critical point. An interaction between two attractors (normally the nuclei) results in a path of maximum electron density between the two attractors. On this line there is a (3,−1) critical point, a so-called bond critical point due to its origin. The Laplacian of the critical point is the sum of the three eigenvalues of the Hessian matrix, λ_1, λ_2, and λ_3. A negative Laplacian in the bond critical point arises when the two atoms share the electron density and is therefore called a "shared interaction". An electrostatic interaction results in a positive Laplacian in the bond critical point, a so-called "closed-shell interaction".

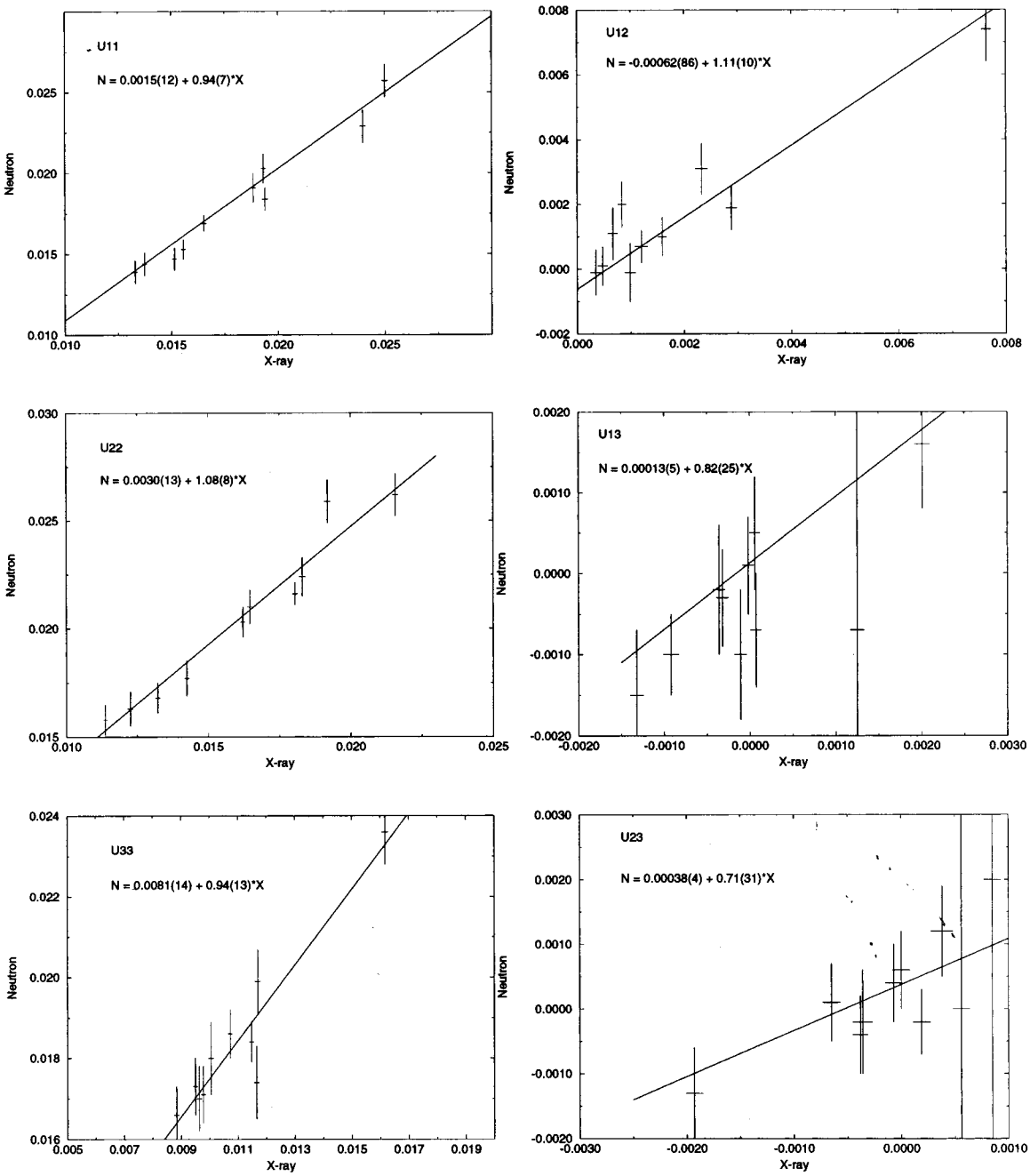

Figure 2. Scaling of anisotropic displacement parameters. The error bars correspond to 1 su. Units on all axes are Å^2.

The deviation from rotation symmetry in the bond is quantified by the ellipticity of the electron density in the bond critical point. With an ordering of the eigenvalues of the Hessian matrix from smallest to largest, the ellipticity is defined as $\lambda_1/\lambda_2 - 1$. An additional strength of the topological analysis is that it enables the definition of atoms within a total density. Atoms separated by the "zero-flux surface" obey quantum chemical and physical relations. The zero-flux surface, S, is defined as $\nabla\rho(\mathbf{r})\cdot\mathbf{n}(\mathbf{r}) = 0$, for all $\mathbf{r}\epsilon S$, where $\mathbf{n}(\mathbf{r})$ is a vector normal to the zero-flux surface. The atomic basins confined by the zero-flux surface and its attractor (normally the nucleus) define an atom in a molecule or crystal, and integration of the Laplacian over an atomic basin should be zero.

For theoretical electron densities the topological analysis is well-established with the appropriate software developed. There is an increasing interest in performing a topological analysis also for experimental charge densities, but the procedures and software employed for the theoretical densities are not directly applicable for the experimental results. Software is available to localize and characterize the critical points in the experimental electron density,[26] but it does not yet contain the algorithms to calculate the zero-flux surfaces that enable the definitions of atoms in the crystal and the subsequent calculation of the atomic properties by integration.

Two recently developed algorithms[27] were used to locate the critical points, to determine the zero-flux surfaces, and to perform the integration in the atomic basins. As an estimate of the accuracy, summations were made of the populations and volumes for the atomic basins in the unit cell; they resulted in values that agreed within 0.3% with $F(000)$ and V_C.

Assuming that the critical points are separated by more than 0.1 Å, a grid of 0.1 Å was used in the search for critical points in the asymmetric unit of the crystal electron density. This resulted in 20 $(3,-3)$ critical points, maxima corresponding to

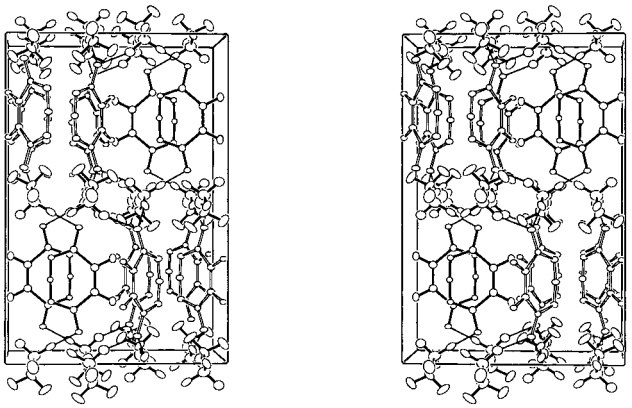

Figure 3. Crystal packing of methylammonium hydrogen maleate viewed along the crystallographic *a*-axis. The *c*-axis is vertical, and the *b*-axis is horizontal. The anion (C(1), C(2), O(1), O(2), H(2), D(2)) is illustrated with open bonds. The thermal ellipsoids scaled to include 50% probability are based on the same parameters as in Figure 1. The hydrogen bonds are shown as thin lines.

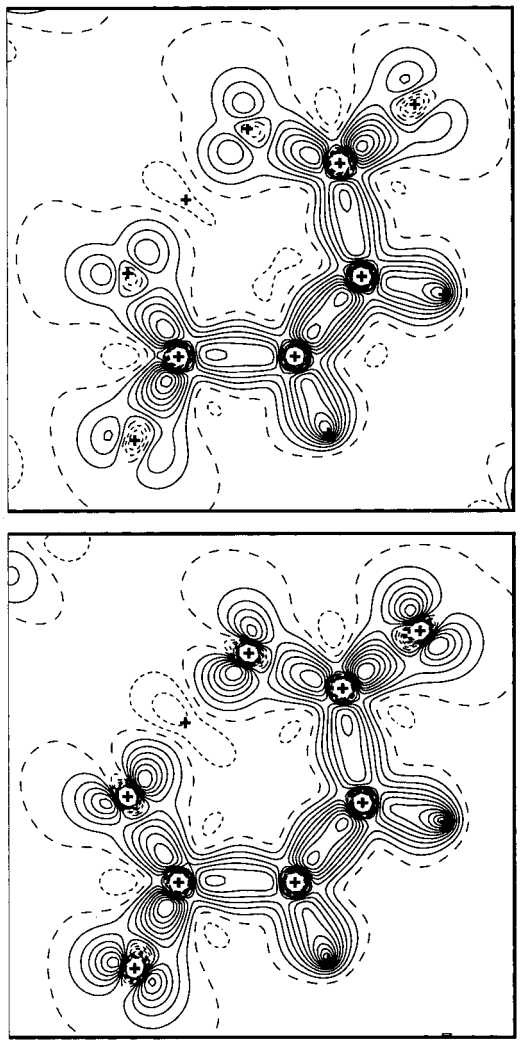

Figure 4. Static deformation maps ($\rho_c - \rho_{IAM}$) shown in the plane of the C atoms in each of the anions (anion 1: C(1), C(2), O(1), O(2), H(2), and D(2) on top). Negative values have broken contours: the long dashed contour is the zero contour. Contour levels are at 0.1 e Å^{-3}. The distance from the O atoms to the least-squares plane is 0.23 Å in anion 1 and 0.05 Å in anion 2. The map sizes are 6.5 Å × 6.5 Å. The positions of the atoms are marked with "+"s.

the atomic positions, 36 (3,−1) bond critical points, 30 (3,1) ring critical points, and 12 (3,3) critical points corresponding

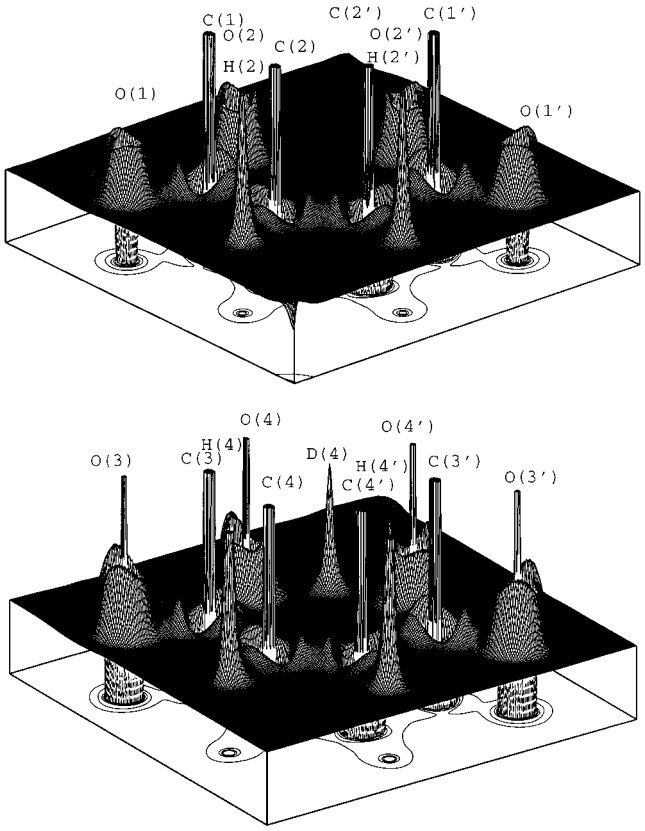

Figure 5. Maps of $-\nabla^2\rho$ shown in the plane of the C atoms in each of the anions. The distance from the O atoms to the least-squares plane is 0.23 Å in anion 1 and 0.05 Å in anion 2. The positive values are truncated at 256 e/Å^5 and negative at −128 e/Å^5. The map sizes are 6.5 Å× 6.5 Å.

to minima. The number of critical points in a unit cell should satisfy the Poincaré−Hopf relation:[28]

$$n(3,-3) - n(3,-1) + n(3,+1) - n(3,+3) = 0$$

where $n(3,i)$ describes the number of $(3,i)$ critical points in the unit cell. Employing the crystallographic symmetry the following numbers were obtained for the critical points in the electron density of the unit cell.

$$152 - 274 + 202 - 80 = 0$$

This demonstrates that the experimentally determined electron density for methylammonium hydrogen maleate fulfills the Poincaré−Hopf relation.

A non-negative crystal electron density is not ensured with the multipole model.[2] We find in all the located minima that $\rho(\mathbf{r}_c) \geq 0$, which implies that the multipole expansion of the experimental electron density does not become negative. Both the fulfillment of the Poincaré−Hopf relation and the non-negativity of the electron density demonstrate that the experimental electron density qualifies for a more thorough analysis. Paths from the bond critical points to the maxima (bond paths) and from the ring critical points to the minima could be traced; thus the topological space found possesses an inner consistency. The lengths of the bond paths are close to the respective interatomic distances.

Hydrogen Maleate Ions. Maps of the negative Laplacian of the electron density in the planes of the carbon skeleton in each of the two anions are shown in Figure 5. Whereas the deformation densities in Figure 4 were very similar, the difference in planarity of the two anions appears clearly in the

TABLE 4: Intramolecular Bond Critical Points in the Hydrogen Maleate Ions[a]

bond, D, $D1$, $D2$ (Å)	$\rho(\mathbf{r}_c)$ (e Å^{-3})	$\nabla^2\rho(\mathbf{r}_c)$ (e Å^{-5})	$\lambda_1, \lambda_2, \lambda_3$ (e Å^{-5})	bond, D, $D1$, $D2$ (Å)	$\rho(\mathbf{r}_c)$ (e Å^{-3})	$\nabla^2\rho(\mathbf{r}_c)$ (e Å^{-5})	$\lambda_1, \lambda_2, \lambda_3$ (e Å^{-5})
C(1)−C(2)	1.84(2)	−12.8(6)	−13.9(3)	C(3)−C(4)	1.82(2)	−12.4(6)	−13.8(4)
1.4921(4)	ellipticity	0.16(3)	−12.0(2)	1.4944(4)	ellipticity	0.16(4)	−11.9(2)
0.754(3)			13.2(1)	0.757(4)			13.2(1)
0.738(3)				0.738(4)			
C(2)−C(2)′	2.37(2)	−20.1(7)	−19.2(4)	C(4)−C(4)′	2.36(2)	−19.7(8)	−18.8(4)
1.3439(3)	ellipticity	0.30(5)	−14.7(3)	1.3446(3)	ellipticity	0.27(4)	−14.9(3)
0.6722(2)			13.9(2)	0.6725(2)			13.9(2)
0.6722(2)				0.6725(2)			
C(1)−O(1)	2.90(2)	−32.8(11)	−27.3(6)	C(3)−O(3)	2.92(2)	−33.3(12)	−27.7(6)
1.2454(3)	ellipticity	0.11(3)	−24.7(4)	1.2433(4)	ellipticity	0.12(3)	−24.7(4)
0.502(5)			19.2(4)	0.499(5)			19.1(4)
0.743(5)				0.745(5)			
C(1)−O(2)	2.64(2)	−28.6(12)	−24.1(6)	C(3)−O(4)	2.60(2)	−28.9(12)	−23.8(6)
1.2817(5)	ellipticity	0.09(3)	−22.0(4)	1.2861(4)	ellipticity	0.11(3)	−21.5(4)
0.513(4)			17.4(4)	0.508(6)			16.4(4)
0.769(4)				0.778(6)			
C(2)−H(2)	1.91(3)	−19.3(9)	−18.6(4)	C(4)−H(4)	1.92(2)	−19.7(8)	−18.5(4)
1.084(5)	ellipticity	0.04(3)	−17.9(4)	1.086(4)	ellipticity	0.04(3)	−17.8(3)
0.714(4)			17.2(2)	0.707(5)			16.6(2)
0.369(6)				0.379(6)			
O(2)−D(2)	1.13(2)	−5.9(9)	−13.3(4)	O(4)−D(4)	1.09(2)	−7.1(9)	−13.8(4)
1.2134(6)	ellipticity	0.00(4)	−13.3(4)	1.2101(5)	ellipticity	0.05(5)	−13.2(4)
0.8994(6)			20.8(3)	0.9160(6)			19.9(3)
0.314(6)				0.294(6)			
anion ring	0.089(5)	1.82(3)	−0.25(2)	anion ring	0.082(5)	1.80(4)	−0.22(3)
			0.86(4)				0.84(4)
			1.21(3)				1.18(3)
C−C (ethylene)[b]	2.451	−28.73	−19.7				
1.317	ellipticity	0.47	−13.6				
0.659			4.6				
C−C (ethane)[b]	1.702	−15.94	−11.5				
1.527	ellipticity	0.00	−11.5				
0.764			7.1				

[a] D is the bond length, $D1$ is the perpendicular distance from the bond critical point to the first atom, and $D2$ to the second atom. λ_1, λ_2, and λ_3 are the three eigenvalues of the Hessian matrix ordered from lowest to highest eigenvalue. The ellipticity is defined as $\lambda_1/\lambda_2 - 1$. [b] The topological features for the C−C bonds in ethylene and ethane are taken from ref 31.

$-\nabla^2\rho$ maps by the visibility of the K shells of the atoms O(3), O(4), and D(4) in the more planar anion. The two maps are very similar in the other regions of the anions. The L shells of the C and O atoms show the expected charge concentrations in the direction of their bonds. The characteristics of the intramolecular bond critical points in the two anions are listed in Table 4, which shows that the two independent anions have almost identical topological features.

The bonds C(2)−C(2)′ and C(4)−C(4)′ are formally double bonds and C(1)−C(2) and C(3)−C(4) single bonds. Despite the fairly large standard uncertainties on the bond ellipticities, an inspection of Table 4 shows that the ellipticities in the bond critical points are larger in the formal double bonds than in the single bonds. It has been demonstrated that the magnitude of the electron density in a bond critical point is related to the bond order.[29,30] Bader et al.[31] found the following relation between the canonical bond orders, n, of the C−C bonds in ethane, ethylene, and acetylene and associated electron density in the bond critical point $\rho(\mathbf{r}_c)$:

$$n = \exp(0.957(\rho(\mathbf{r}_c) - 1.70))$$

We have used this expression to estimate the C−C bond orders in the two hydrogen maleate ions. Using the values for $\rho(\mathbf{r}_c)$ from Table 4 leads to the following bond orders for the C−C bonds: n(C(2)−C(2)′) = 1.90(4), n(C(4)−C(4)′) = 1.88(4), n(C(1)−C(2)) = 1.14(2), and n(C(3)−C(4)) = 1.12(2). Despite the small difference in the planarity of the anions, they have identical bond orders that show the expected conjugation of the hydrogen maleate ion.

For comparison Table 4 also contains information on the topological features obtained from theoretical calculations for ethane and ethylene.[31] The excellent agreement between theoretical and experimental estimates of $\rho(\mathbf{r}_c)$ and the two negative eigenvalues of the Hessian matrix (λ_1 and λ_2) is not found for the positive λ_3, where significantly smaller values are found in the theoretical calculations. Similar discrepancies between experimental and theoretical values of λ_3 were observed earlier in the study of L-dopa.[6] This is an effect of placing the molecules in a crystal lattice, as it is also seen in periodic Hartree−Fock calculations.[32] The higher electrostatic pressure in the crystal electron density is expected to compress the more diffuse electron density outside the bond path more than in the bond path and therefore to affect the value of $\nabla^2\rho(\mathbf{r}_c)$ to a much larger extent than $\rho(\mathbf{r}_c)$.

The C−O bonds in the carboxy groups show the expected property of one bond being significantly stronger (higher $\rho(\mathbf{r}_c)$) than the other. They have very small ellipticities that are identical within the standard uncertainty. The topological properties of the C−O bond critical points are in good agreement with the characteristics of the C−O bond critical points derived from other experimental electron density studies.[3,4] When the variation of the C−O bond length is taken into account, as Roversi et al.[4] did in their study of citrinin, an even better agreement for $\rho(\mathbf{r}_c)$ is obtained. For the C−O bonds they found the following relation between the electron density in the critical point and the bond length:

$$\rho(\mathbf{r}_c) = 8.433R_b^{-3.521}$$

TABLE 5: Integrated Laplacian (L), Volume (V), Charge (q) and Quadrupole Moment Component Q_{zz} of the Atomic Basins in the Anions[a]

Ω	$L \times 10^3$/(e Å^{-2})	V/Å^3	q(Ω)/e	q(mp)/e	Q_{zz}/(e Å^2)
C(1)	−3.1	5.90	1.23	0.00(2)	0.11
C(2)	−2.9	12.51	−0.11	−0.07(3)	0.24
O(1)	3.9	17.11	−1.00	−0.33(3)	0.17
O(2)	1.8	18.00	−1.04	−0.31(3)	0.03
H(2)	6.5	6.24	0.14	0.07(2)	0.00
D(2)	7.2	1.01	0.66	0.37(2)	0.02
Σ(COO$^-$)		41.01	−0.81	−0.64(5)	0.31
Σ(CH)		18.75	0.03	0.00(4)	0.24
Σ(anion1)		120.53	−0.90	−0.91(9)	1.12
C(3)	−2.9	5.73	1.27	0.02(2)	0.12
C(4)	−3.3	11.99	−0.11	−0.04(3)	0.25
O(3)	2.2	17.55	−0.98	−0.30(3)	0.17
O(4)	1.7	16.36	−1.03	−0.33(3)	0.02
H(4)	7.2	5.98	0.13	0.06(2)	−0.01
D(4)	6.9	0.85	0.71	0.45(2)	0.02
Σ(COO$^-$)		39.64	−0.74	−0.61(5)	0.31
Σ(CH)		17.97	0.02	0.02(4)	0.24
Σ(anion2)		116.07	−0.73	−0.73(9)	1.12

[a] The number of points determined on the zero-flux surface for each atomic basin for the C and O atoms is 2788 with ca. 500 000 integration points in each basin. The corresponding numbers for the H/D atomic basins are 650 and 250 000. $q(mp)$ is calculated from the population of the monopole parameter from the refinement of the X-ray data.

($\rho(\mathbf{r}_c)$ is in the units e/(au)^3 and R_b in bohr). If we insert the experimental bond lengths into this expression, the following values are obtained: $\rho(\mathbf{r}_c)$(C(1)−O(1)) = 2.80, $\rho(\mathbf{r}_c)$(C(1)−O(2)) = 2.53, $\rho(\mathbf{r}_c)$(C(3)−O(3)) = 2.81, $\rho(\mathbf{r}_c)$(C(3)−O(4)) = 2.50 e Å^{-3}; they correspond well to the values listed in Table 4.

Most of the ring critical points located in the unit cell are intermolecular, with small values of $\rho(\mathbf{r}_c)$ and $\nabla^2\rho(\mathbf{r}_c)$. In each of the hydrogen maleate ions an intramolecular ring critical point is found (cf. Table 4). Their topological properties are identical within the standard uncertainties, and they have values of $\rho(\mathbf{r}_c)$ that are ca. 10 times higher than the $\rho(\mathbf{r}_c)$ of the other ring critical points.

Table 5 contains information of some of the properties of the atoms in the anions obtained by integration over the atomic basins.[27] The values for the integrated Laplacian are sufficiently close to 0 that it gives faith in the physical content of the other integrated properties. The integrated quadrupole moment of the atomic basin is related to the π character of the bonds that the atom takes part in.[33,34] The orthogonal coordinate system used in the multipole description is aligned with its z-axis parallel to the crystallographic c-axis. As mentioned earlier and illustrated in Figure 3, we find that the two anions are oriented in the crystal with the c-axis virtually in their molecular planes. We would therefore expect that a larger Q_{zz} component would reflect a depletion of charge in the planes of the anions. Inspection of the Q_{zz} values in Table 5 reveals that high values are found at the C atoms, with the maximum values at C(2) and C(4). The atoms O(1) and O(3) have large Q_{zz} components indicating that the bonds C(1)−O(1) and C(3)−O(3) have bond orders above 1, whereas the Q_{zz} components for O(2) and O(4) have values close to 0, indicating C(1)−O(2) and C(3)−O(4) are single bonds, in agreement with the bond lengths given in Table 4.

This makes us conclude that the conjugated system in the hydrogen maleate ion includes the carbon skeleton and the double-bonded O atoms, but not the oxygen atoms linked by the very short intramolecular hydrogen bond. The calculated integrated properties of the individual atomic basins and the chemical functional groups are transferable between the two hydrogen maleate ions, and the total charges of −0.90e and −0.73e are not grossly different from the formal value of −1e.

Very Short O−H−O Hydrogen Bonds. In the study of the equivalent hydrogen succinate salt it was demonstrated that a very short intermolecular O−H−O hydrogen bond possesses covalent character.[3] In that case the short hydrogen bond was between two different anions related by a crystallographic inversion center. The topological properties of the bond critical points in the very short symmetric O−H−O intramolecular hydrogen bonds (O(2)−D(2) and O(4)−D(4)) are shown in Table 4. The two symmetric intramolecular hydrogen bonds have very similar characteristics. The critical points are found at the same distance ca. 0.30 Å from the H/D atom, and the negative values of their Laplacians show the covalent character of the intramolecular hydrogen bond. Both the relative position and the numerical values of $\rho(\mathbf{r}_c)$ and $\nabla^2\rho(\mathbf{r}_c)$ are virtually identical to those found for the critical point that represents the short symmetrical intermolecular hydrogen bond in MAHS.[3] The values of $\rho(\mathbf{r}_c)$ are much higher than the ones reported for normal hydrogen bonds[1] and correspond to 40% of $\rho(\mathbf{r}_c)$ in the O−H covalent bond in H_2O (value 2.63 e Å^{-3} taken from Bader[1]). The interactions are so strong that D(2) and D(4) are significantly depleted of electrons, as integration of the charge in the atomic basins gives +0.66e and +0.71e for D(2) and D(4), respectively.

The topological analysis of the two hydrogen maleate ions has also shown that the conjugated part of these anions did not include the short hydrogen bond. In view of this result we would expect that the intramolecular very short hydrogen bonds would be similar to the equivalent intermolecular interactions in the hydrogen succinate salt. This can explain the equivalence between the properties of their bond critical points.

To further characterize D(2) and D(4) in the short hydrogen bonds, the electrostatic potential in the unit cell was mapped out on the basis of the F_c models.[35] This is done by a combination of Fourier and direct space lattice sums as described in greater detail in the similar investigation of MAHS.[3] In this latter study the potential in the crystal was calculated with the potential due to the hydrogen atom in the short hydrogen bond removed. The resulting potential showed a distinct local minimum, at the special position (inversion center) where the proton is located. We found it of interest to examine whether similar single-well potentials exist for the protons in the short intramolecular hydrogen bonds of the hydrogen maleate ions. Maps of the electrostatic potential calculated without the contributions from D(2) and D(4) in the short hydrogen bonds are shown in Figure 6, which both show one distinct minimum. The largest curvature of the potential is in both cases in the direction of the respective O atoms. A crude estimate of the electrostatic energy of stabilization can be obtained by multiplication of the charges in the multipole model of the removed atoms and the minima in the potential when their potentials have been subtracted. The monopole charges of D(2) and D(4) are +0.37e and +0.45e, respectively, and the minima have values of −13.1 and −14.3 V (−0.91 and −0.99 e/Å). Placing the protons in their respective minima gives the energies 4.9 and 6.4 eV (473 and 617 kJ/mol) that at least are of the right order of magnitude.

The Methylammonium Ion and Transferability of Topological Properties. A map of the negative Laplacian in the plane of N(1), C(5), and H(7) is shown in Figure 7. The L shells of N(1) and C(5) show charge concentrations directed toward their bonds. Although there is no crystallographic symmetry imposed on the cation, it possesses almost a mirror

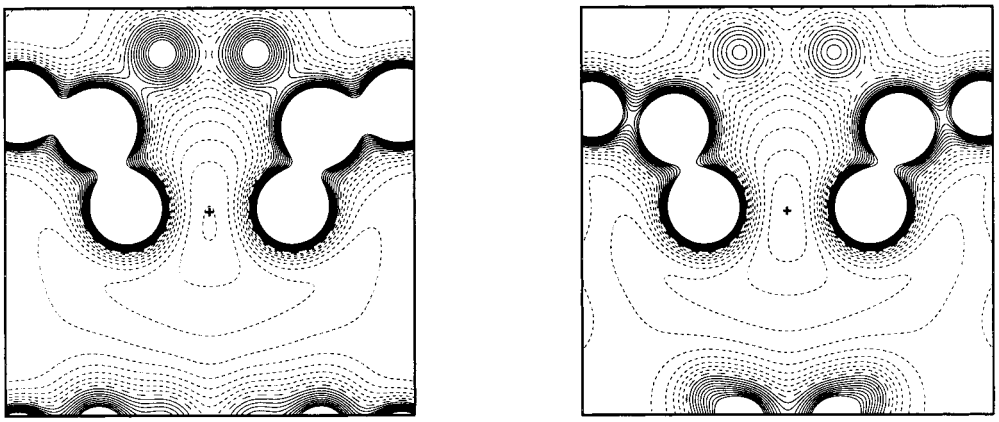

Figure 6. Crystal electrostatic potential in the plane with the largest gradient of the very short symmetric hydrogen bonds (D(2) on the left) with the potential of D(2) and D(4) respectively removed. The contours of constant equipotential are in units of e/Å with a difference of 0.1 e/Å between the lvels. The maximum contour for D(2) and D(4) correspond to +0.90 and +0.99 e/Å, respectively. Short dashed lines indicate negative potential; the long dashed line is the zero-potential line.

TABLE 6: Intramolecular Bond Critical Points of the Methylammonium Ion in MADMA and MAHS[a]

MADMA				MAHS			
bond, *D*, *D*1, *D*2 (Å)	$\rho(\mathbf{r}_c)$ (e Å^{-3})	$\nabla^2\rho(\mathbf{r}_c)$ (e Å^{-5})	$\lambda_1, \lambda_2, \lambda_3$ (e Å^{-5})	bond, *D*, *D*1, *D*2 (Å)	$\rho(\mathbf{r}_c)$ (e Å^{-3})	$\nabla^2\rho(\mathbf{r}_c)$ (e Å^{-5})	$\lambda_1, \lambda_2, \lambda_3$ (e Å^{-5})
C(5)−N(1)	1.73(2)	−8.4(7)	−11.4(3)	C(3)−N(1)	1.63(2)	−12.1(8)	−10.0(4)
1.4807(6)	ellipticity	0.00(4)	−11.3(3)	1.4798(17)	ellipticity	0.01(5)	−9.9(3)
0.638(6)			14.4(2)	0.590(12)			7.8(2)
0.842(6)				0.890(12)			
C(5)−H(5)	1.86(2)	−17.1(8)	−17.3(4)	C(3)−H(6)	1.92(2)	−20.1(7)	−18.3(3)
1.077(5)	ellipticity	0.04(3)	−16.7(4)	1.076(3)	ellipticity	0.04(3)	−17.5(4)
0.703(5)			16.9(2)	0.692(4)			15.7(2)
0.383(6)				0.384(4)			
C(5)−H(6)	1.97(3)	−21.6(10)	−18.9(4)	C(3)−H(7)	1.93(2)	−20.3(9)	−18.0(4)
1.084(5)	ellipticity	0.02(3)	−18.6(4)	1.072(5)	ellipticity	0.02(3)	−17.7(4)
0.705(6)			16.0(2)	0.684(8)			15.3(2)
0.379(6)				0.389(8)			
C(5)−H(7)	1.97(2)	−21.7(8)	−18.9(4)				
1.086(6)	ellipticity	0.02(3)	−18.5(4)				
0.700(4)			15.7(2)				
0.377(6)							
N(1)−D(5)	2.12(3)	−31.1(16)	−29.0(7)	N(1)−H(4)	2.13(4)	−35.5(16)	−29.1(7)
1.038(3)	ellipticity	0.03(3)	−28.2(7)	1.031(3)	ellipticity	0.02(4)	−28.6(7)
0.782(3)			26.0(4)	0.783(3)			22.2(3)
0.257(6)				0.249(3)			
N(1)−D(6)	2.13(3)	−31.1(16)	−29.2(7)	N(1)−H(5)	2.10(4)	−36.0(18)	−29.1(8)
1.038(3)	ellipticity	0.02(4)	−28.7(7)	1.039(6)	ellipticity	0.03(4)	−28.2(8)
0.775(3)			26.7(5)	0.793(6)			21.4(5)
0.252(6)				0.246(4)			
N(1)−D(7)	2.19(3)	−33.8(16)	−29.7(7)				
1.027(3)	ellipticity	0.02(4)	−29.2(7)				
0.773(3)			25.1(4)				
0.266(6)							

[a] *D* is the bond length, *D*1 is the perpendicular distance from the critical point to the first atom, and *D*2 to the second atom. λ_1, λ_2, and λ_3 are the three eigenvalues of the Hessian matrix ordered from lowest to highest eigenvalue. The ellipticity is defined as $\lambda_1/\lambda_2 - 1$.

plane, which makes D(6) visible in the plane defined by N(1), C(5), and H(7). This symmetry facilitates the comparison with the results of the same cation in the hydrogen succinate salt, where it was found on a crystallographic mirror plane. The integrated volumes, charges, and Laplacians of the atomic basins in the methylammonium ions are listed in Table 7. It should be noted that the two values for the integrated charge of the cation (+0.88*e* and +0.99*e*) are close to the formal value of +1*e*.

The ammonium group of the cation in the hydrogen maleate salt (MADMA) is hydrogen-bonded by three different hydrogen maleate ions. In methylammonium hydrogen succinate monohydrate all possible donor atoms are also involved in hydrogen bonds, the ammonium group is hydrogen-bonded to a water molecule, and the C═O groups from two anions are related by the mirror plane symmetry.[3] In both salts these hydrogen bonds are normal, with N···O distances in the range 2.7−2.9 Å. The intramolecular critical points of the methylammonium ion in MADMA and MAHS are listed in Table 6; the atomic labels in this table refer to Figure 8. A high degree of transferability of the properties of the methylammonium ion between these two compounds could be expected due to the similarities in the hydrogen-bonding environment. As a consequence of the crystallographic mirror plane in the cation in MAHS, the number of unique C−H and N−H bonds is reduced by one, but the properties of the equivalent critical points are identical within 5 su. In a study of the charge density of peptide-like molecules it was found that the multipole parameters were transferable.[36] A more quantitative study of the transferability of properties derived from the total electron density of related molecules has

TABLE 7: Values of the Integrated Laplacian (*L*), volume (*V*), and Charge (*q*) of the Atomic Basins of the Cation in MADMA and MAHS[a]

Ω	L × 10^3/e Å^{-2}	*V*(Ω)/Å^3	*q*(Ω)/e	*q*(mp)/e
		MADMA		
C(5)	−6.3	11.1	0.00	0.04(4)
N(1)	−4.7	13.9	−1.14	−0.02(6)
D(5)	3.7	2.2	0.52	0.22(2)
D(6)	6.2	2.6	0.52	0.22(2)
D(7)	5.4	1.9	0.52	0.18(2)
H(5)	3.5	5.8	0.12	0.06(2)
H(6)	4.5	5.5	0.16	0.06(2)
H(7)	3.1	5.4	0.17	0.06(2)
$\sum(CH_3)$		27.8	0.45	0.22(5)
$\sum(NH_3)$		20.6	0.42	0.60(7)
$\sum(CH_3NH_3^+)$		48.4	0.88	0.82(9)
		MAHS		
C(3)	−6.8	11.3	0.12	−0.12(5)
N(1)	−15.8	13.9	−1.25	0.05(6)
H(4)	7.5	2.1	0.55	0.19(2)
H(5)	7.0	1.8	0.59	0.22(2)
H(6)	8.6	6.4	0.15	0.14(2)
H(7)	8.6	7.8	0.13	0.12(2)
$\sum(CH_3)$		31.9	0.55	0.38(6)
$\sum(NH_3)$		19.9	0.44	0.65(7)
$\sum(CH_3NH_3^+)$		51.0	0.99	1.03(9)

[a] The integration of the atomic basins has the same accuracy as the atomic basins in the anions in MADMA. *q*(mp) is calculated from the population of the monopole parameter from the refinement of the X-ray data.

been carried out by Espinosa et al.[37] The present study represents the first thorough investigation of the same molecular entity in slightly different environments.

The integrated properties of the basins in the methylammonium ion in the two compounds (cf. Table 7) are transferable between chemically equivalent atomic basins, of the chemical functional groups and of the whole fragment. These comparisons show that quantitative transferability of topological features is applicable to experimentally determined electron densities.

Atomic Charges from Diffraction Data. The charges calculated from the zero-flux surface partitioning indicate a larger charge transfer between the atoms than other charge partitioning schemes, i.e. like the summation of monopole populations in Tables 5 and 7. The same differences have been observed in the zero-flux partitioning of theoretical charge densities.[38] The charges of molecular fragments of the electron density from the two partitioning schemes are almost identical. We attribute this agreement to the very low electron density between the fragments.

The higher moments of the electron density (e.g., the dipole moments and quadrupole moments) are quite different from the values obtained from the multipole parameters, as exemplified by the magnitude of the dipole moment for anion 1 (C(1), C(2), O(1), O(2), D(2), H(2)), which is 0.25(25) e Å derived from the multipole model and 0.88 e Å derived from the integrated properties. The center of mass in the anion was used as the origin in both calculations. The angle between the dipole moments derived from the multipole model and the integrated properties is 55°, where the direction of the dipole moment derived from the integrated properties is in the plane of the anion pointing away from the carboxylate groups, as expected. It would be of interest to elucidate this aspect further by other types of calculations and experiments.

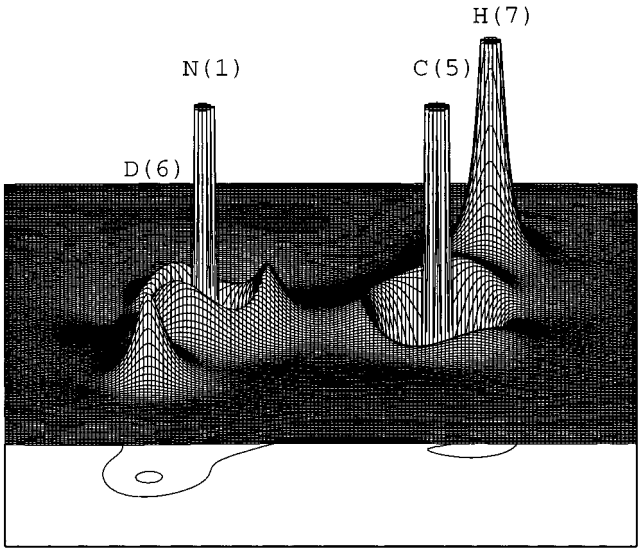

Figure 7. Map of $-\nabla^2\rho$ in the plane of N(1), C(5), and H(7). D(6) is 0.1 Å from the plane. The positive values are truncated at 256 e/Å^5 and negative at −128 e/Å^5. The map size is 4.0 Å × 4.0 Å.

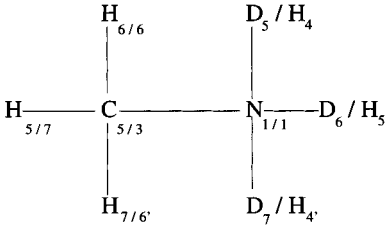

Figure 8. Methylammonium ion with the labeling of the atoms in MADMA and MAHS. The notation $C_{5/3}$ indicates that C has number five in MADMA and three in MAHS.

N−H···O Hydrogen Bonds. The previous structural study of MADMA had identified three intermolecular N−H···O hydrogen bonds on the basis of geometrical criteria.[10] The

TABLE 8: Intermolecular Bond Critical Points and Geometry of the N−H···O Hydrogen Bonds[a]

bond, *D*1, *D*2 (Å)	$\rho(\mathbf{r}_c)$ (e Å^{-3})	$\nabla^2\rho(\mathbf{r}_c)$ (e Å^{-5})	$\lambda_1, \lambda_2, \lambda_3$ (e Å^{-5})	geometry (Å) and (deg)	
O(1)···D(5)	0.24(1)	2.1(2)	−1.6(1)	N(1)−D(5)	1.038(3)
	ellipticity	0.12(8)	−1.4(1)	N(1)···O(1)^i	2.8372(5)
1.182(7)			5.1(1)	D(5)···O(1)$^{i\ b}$	1.834(3)
0.656(12)				N(1)−D(5)···O(1)^i	161.2(3)
O(1)···D(6)	0.19(1)	2.0(1)	−1.1(1)	N(1)−D(6)	1.027(3)
	ellipticity	0.06(10)	−1.0(1)	N(1)···O(1)	2.8972(6)
1.218(10)			4.2(1)	D(6)···O(1)	1.910(3)
0.694(10)				N(1)−D(6)···O(1)	160.2(3)
O(3)···D(7)	0.29(1)	1.7(2)	−2.0(1)	N(1)−D(7)	1.039(3)
	ellipticity	0.10(8)	−1.8(1)	N(1)···O(3)	2.8188(6)
1.163(6)			5.6(1)	D(7)···O(3)	1.792(3)
0.629(9)				N(1)−D(7)···O(3)	169.2(3)

[a] D1 is the distance from the critical point to the first atom and D2 to the second atom. λ_1, λ_2 and λ_3 are the three eigenvalues of the Hessian matrix ordered from lowest to highest eigenvalue. The ellipticity is defined as $\lambda_1/\lambda_2 - 1$.

ammonium group is hydrogen-bonded to three C−O groups, two from the less planar (O(1)) and one from the more planar (O(3)) anion. These intermolecular interactions were found in the topology of the crystal electron density as three bond critical points by tracing the bond paths (cf. Table 8). The topological properties are as expected for regular hydrogen bonds and compare well with the equivalent values in MAHS. The $\rho(\mathbf{r}_c)$ values for the three N−H···O hydrogen bonds in MADMA (Table 8) show a systematic decrease with the hydrogen acceptor distance. A similar systematic variation is not found for the Laplacians, which are all close to 2.0 e Å^{-5} within 2 su, but leaves no doubt that these interactions are electrostatic (closed shell) in nature. The three hydrogen bonds are of the normal linear type, so short hydrogen acceptor distances are associated with short donor−acceptor distances. It has been demonstrated earlier that the electron density at the critical point $\rho(\mathbf{r}_c)$ reflects the strength (energy) of the hydrogen bond.[30] Therefore it can be concluded that the general assumption on hydrogen bond strengths, i.e. that stronger hydrogen bonds have shorter donor−acceptor distance and are more linear, is supported by the findings for these three N−H···O hydrogen bonds.

The charge transfer due to hydrogen bonding has been shown by theoretical calculations to be small but detectable.[30] We would therefore expect that the integrated charges of the crystal electron density should be close to those found in the non-hydrogen-bonded fragments. The integrated charges of the O atoms and the N atom are close to $-1e$, and the integrated charges of the H/D atoms are $+0.5e$ to $+0.7e$. A simple electrostatic description for the O−H−O and the N−H···O hydrogen bonds has negative donor and acceptor atoms and a positive H/D atom, $D^{-}-H^{+}\cdots A^{-}$, whereas a neutral nitrogen atom is deduced from the multipole populations.

Other Bond Critical Points. Half of the (3,−1) critical points located in the asymmetric unit have been listed in the previous tables. The remaining bond critical points can be attributed to C−H···O interactions and intermolecular interactions between non-H/D atoms or H−H repulsions. Whether the interactions between non-H/D atoms are due to artifacts of the multipole model or errors in the determined electron density or have physical significance should be elucidated further before they are discussed in greater details.

Conclusions

The topological analysis of the experimental electron density in methylammonium hydrogen maleate showed that it constitutes a topological space that satisfies the Poincaré−Hopf relation, and the electron density is positive throughout the unit cell.

The bond critical points in chemically equivalent bonds have identical topological properties within the standard uncertainty (cf. Tables 4 and 6), which is another indication of the physical significance of this experimental electron density. The topological analysis showed that the very short intramolecular O−H−O hydrogen bonds in the hydrogen maleate ions possess covalent character. This is in agreement with the results obtained for the short intermolecular hydrogen bond in the hydrogen succinate salt showing that covalency is the dominant feature for very short hydrogen bonds.

A comparison of the methylammonium ion in the two different salts has shown that all the properties of critical points as well as the integrated properties of the atomic basins are transferable.

Acknowledgment. The authors are grateful to Professor Robert F. Stewart for his inspiration and interest in this work. We thank Mr. Henrik Birkedal for discussions and careful reading of the manuscript. The help from Mr. Flemming Hansen in connection with the X-ray and neutron data collections and from Dr. Pernille Harris during the neutron data collection is gratefully acknowledged. We thank Dr. Bente Lebech for providing the measuring time at the TAS2 diffractometer at the DR3 reactor at Risø National Laboratory. The Centre for Crystallographic Studies is funded by the Danish National Research Foundation.

Supporting Information Available: Difference density map of the region around one of the anions (1 page). Lists of observed and calculated structure amplitudes will appear in the microfiche version only. Ordering information is given on any current masthead page.

References and Notes

(1) Bader, R. F. W. *Atoms in Molecules−A Quantum Theory*; Oxford University Press: Oxford, 1994.
(2) Stewart, R. F. In *The Application of Charge Density Research to Chemistry and Drug Design*; Jeffrey, G., Piniella, J., Eds.; Plenum Press: New York, 1991; p 63.
(3) Flensburg, C.; Larsen, S.; Stewart, R. F. *J. Phys. Chem.* **1995**, *99*, 10130.
(4) Roversi, P.; Barzahgi, M.; Merati, F.; Destro, R. *Can. J. Chem.* **1996**, *74*, 1145.
(5) Koritsanszky, T.; Buschmann, J.; Luger, P. *J. Phys. Chem.* **1996**, *100*, 10547.
(6) Howard, S. T.; Hursthouse, M. B.; Lehmann, C. W.; Poyner, E. A. *Acta Crystallogr.* **1995**, *B51*, 328.
(7) Tuckerman, M. E.; Marx, D.; Klein, M. L.; Parrinello, M. *Science* **1997**, *275*, 817.
(8) Gilli, P.; Bertolasi, V.; Ferretti, V.; Gilli, G. *J. Am. Chem. Soc.* **1994**, *116*, 909.
(9) Speakman, J. C. *Struct. Bonding (Berlin)* **1972**, *12*, 141.
(10) Madsen, D.; Larsen, S. *Acta Crystallogr. C*, in press.
(11) Johnson, C. K. *Report ORNL.5138*; Oak Ridge National Laboratory, TN, 1976.
(12) Frazer, B. C.; Pepinsky, R. *Acta Crystallogr.* **1953**, *6*, 273.
(13) Sheldrick, G. M. *Program for the Refinement of Crystal Structures*; University of Göttingen, Germany, 1993.
(14) Blessing, R. H. *Cryst. Rev.* **1987**, *1*, 3.
(15) Stewart, R. F.; Spackman, M. A.; Flensburg, C. *VALRAY Reference Manual* β -version; April 1996.
(16) Hamilton, W. C. *Acta Crystallogr.* **1965**, *A18*, 502.
(17) Koster, L.; Rauch, H.; Herkens, M.; Scröder, K. *Summary of Neutron Scattering Lengths*; KFA: Jülich, Germany, 1981.
(18) Becker, P. J.; Coppens, P. *Acta Crystallogr.* **1974**, *A30*, 129.
(19) Stewart, R. F. *J. Chem. Phys.* **1969**, *51*, 4569.
(20) Stewart, R. F. *Acta Crystallogr.* **1976**, *A32*, 565.
(21) van der Wal, R. J.; Stewart, R. F. *Acta Crystallogr.* **1984**, *A40*, 587.
(22) Clementi, E.; Roetti, C. *Atomic Data Nucl. Data Tables*; 1974, Vol. 14.
(23) Hehre, W. J.; Ditchfield, R.; Stewart, R. F.; Pople, J. A. *J. Chem. Phys.* **1970**, *52*, 2769.
(24) Blessing, R. H. *Acta Crystallogr.* **1995**, *A51*, 33.
(25) Hsu, B.; Schlemper, E. O. *Acta Crystallogr.* **1980**, *B36*, 3017.
(26) Koritsansky, T.; Howard, S. T.; Mallinson, R. P.; Su, Z.; Richter, T.; Hansen, N. K. *XD, A Computer Program Package for Multipole Refinement and Analysis of Charge Densities from X-ray Diffraction Data*; Free University Berlin, 1995.
(27) Flensburg, C.; Madsen, D. *Acta Crystallogr. A.*, to be submitted.
(28) Collard, K.; Hall, G. G. *Int. J. Quantum Chem.* **1977**, *12*, 623.
(29) Boyd, R. J.; Choi, S. C. *Chem. Phys. Lett.* **1986**, *129*, 62.
(30) Carroll, M. T.; Bader, R. F. W. *Mol. Phys.* **1988**, *65*, 695.
(31) Bader, R. F. W.; Slee, T. S.; Cremer, D.; Kraka, E. *J. Am. Chem. Soc.* **1983**, *105*, 5061.
(32) Gatti, C.; Saunders, V. R.; Roetti, C. *J. Chem. Phys.* **1994**, *101*, 10686.
(33) Bader, R. F. W.; Chang, C. *J. Phys. Chem.* **1989**, *93*, 2946.
(34) Bader, R. F. W.; Chang, C. *J. Phys. Chem.* **1989**, *93*, 5095.
(35) Stewart, R. F. *God. Jugosl. Cent. Kristalogr.* **1982**, *17*, 1.
(36) Pichon-Pesme, V.; Lecomte, C.; Lachekar, H. *J. Phys. Chem.* **1995**, *99*, 6642.
(37) Espinosa, E.; Lecomte, C.; Molins, E.; Veintemillas, S.; Coussin, A.; Paulus, W. *Acta Crystallogr.* **1996**, *B52*, 519.
(38) Meister, J.; Schwarz, W. H. E. *J. Phys. Chem.* **1994**, *98*, 8245.